

Quantum probabilistic sampling of multipartite 60-qubit Bell inequality violations

M. D. Reid¹, B. Opanchuk¹, L. Rosales-Zárate¹, P. D. Drummond¹

¹*Centre for Quantum and Optical Science, Swinburne University of Technology, Melbourne 3122, Australia*

We show that violation of genuine multipartite Bell inequalities can be obtained with sampled, probabilistic phase space methods. These genuine Bell violations cannot be replicated if any part of the system is described by a local hidden variable theory. The Bell violations are simulated probabilistically using quantum phase-space representations. We treat mesoscopically large Greenberger-Horne-Zeilinger (GHZ) states having up to 60 qubits, using both a multipartite SU(2) Q-representation and the positive P-representation. Surprisingly, we find that sampling with phase-space distributions can be exponentially *faster* than experiment. This is due to the classical parallelism inherent in the simulation of quantum measurements using phase-space methods. Our probabilistic sampling method predicts a contradiction with local realism of “Schrödinger-cat” states that can be realized as a GHZ spin state, either in ion traps or with photonic qubits. We also present a quantum simulation of the observed super-decoherence of the ion-trap “cat” state, using a phenomenological noise model.

I. INTRODUCTION

Quantum simulation of systems with many degrees of freedom is a difficult and interesting problem of much topical interest. Calculating the dynamics of many-body quantum systems is hard, since the Hilbert space dimension increases exponentially with the number of modes or degrees of freedom [1, 2]. There are two main approaches: one can do a computational simulation [3–8], or else a physical simulation with another quantum system [9–13]. Universal quantum computers provide a third option [14], but these are limited in size.

One path to solving this problem is to use probabilistic simulations whose correlations correspond to quantum averages. For large problems, this approach was pioneered by Glauber and co-authors [3, 15], who studied quantum statistics of super-fluorescence. Later, their approximate method was generalized to an exact probabilistic representation of arbitrary quantum states [16, 17]. Quantum simulation predictions were experimentally verified for multi-mode optical fields displaying squeezing and quantum entanglement [4, 18–20]. More recently, the method has been applied to colliding BEC systems [5, 21], and to Bell violations in parametric down-conversion experiments [22].

Here we study how efficiently such probabilistic methods can be used to simulate the most extreme quantum superposition states – or “Schrödinger cat” states. The “cat” state is often represented as a GHZ state for M particles [23]:

$$|\Phi\rangle = \frac{1}{\sqrt{2}} (|\uparrow \dots \uparrow\rangle + e^{i\phi} |\downarrow \dots \downarrow\rangle). \quad (1)$$

where $|\uparrow \dots \uparrow\rangle = \bigotimes_{j=1}^M |\uparrow\rangle_j$, $|\downarrow \dots \downarrow\rangle = \bigotimes_{j=1}^M |\downarrow\rangle_j$ and $|\uparrow\rangle_j$, $|\downarrow\rangle_j$ are the eigenstates of the spin $\hat{\sigma}^z$ of the j -th particle. A powerful signature of the “cat” state is its M -qubit nonlocality. These have been explored in photonic [24] and ion trap experiments [25], which demonstrated Bell-Mermin violations and genuine M -particle entanglement for up to $M = 14$ ions [26].

We investigate probabilistic methods for simulating both Bell-Mermin violations and the more challenging Svetlichny-Collins genuine Bell violations in these multipartite “cat” states. The latter inequality allows us to demonstrate the genuine M -partite nonlocality of the multipartite GHZ state (1) for up to $M = 60$ ions or modes. This is a true Schrödinger cat signature: it cannot be obtained if any subset has a local hidden variable (LHV) description. It is often thought that probabilistic sampling would be extraordinarily difficult for a “cat” state of large size. Probabilistic methods using measured eigenvalues are impossible, since this would amount to an LHV theory, which cannot violate a Bell inequality.

Importantly, Mermin showed that the difference between LHV predictions and quantum predictions scales exponentially with increasing system size M [27], making this a significant challenge for probabilistic methods. However, the techniques used in this paper do *not* rely on LHV theories, but instead sample over stochastic variables whose values are permitted to go beyond the eigenvalue spectrum. The ability to simulate quantum mechanics in this way gives a beautiful analogy to the theory of weak values and measurements [28], as has been explained elsewhere [22, 29, 30].

We find that sampling errors of high-order correlations are larger than for low-order correlations. We note that M -order correlations are needed to display the signature of an M -partite Bell-Svetlichny nonlocality. However, for these results, phase-space simulations have a classical parallelism not available in any quantum experiment. This parallelism occurs because exponentially many non-commuting measurements can be calculated at once. The result is an exponential *speedup* for simulating multipartite Bell violations. The simulation is $e^{M/3}$ times faster than experiment with methods used here.

The general advantage of probabilistic sampling in quantum simulations compared to wave-function methods [12] is that the required computational memory scales linearly, not exponentially, with the number of qubits. This eliminates the problem of exponential scaling in memory size found in direct, orthogonal basis calcula-

tions. The time taken, or equivalently the number of samples required, depends on the type of measurement and the resulting sampling error in a finite ensemble. We consider the Greenberger-Horne-Zeilinger (GHZ) state (1), and simulate spin correlations as well as multipartite Bell violations.

The utility of phase-space representations is that they provide a route to performing such probabilistic sampling. We employ two common positive phase-space distributions, namely, the SU(2) Q function [31–33] and the positive P-distribution [16]. The latter method has already been used to obtain analytic results for probabilistic Bell violation [34]. To focus on the sampling issue, we mostly treat static cases with known probability distributions. We also treat dynamical simulations of decoherence. A summary of the results is published elsewhere [30].

In these multipartite investigations, we use Bell-like inequalities that extend the usual bipartite inequalities to many qubits. We test the MABK (Mermin-Ardehaly-Belinski-Klyshko) inequality [27, 35–37] which is a Bell inequality generalized to multipartite qubit systems, and the Collins-Svetlichny inequalities [38, 39], which are sufficient conditions for genuine multipartite Bell violations [40–44]. Genuine multipartite Bell violations prove that Bell violations are a macroscopic property.

We find different behavior depending on the order of the correlation function. There is no growth in sampling error with the number of qubits when simulating low-order correlations in our calculations. Thus, fixed order correlations do not have an exponential increase in simulation time. However, correlations with a growing order equal to the number of qubits take an exponentially long time to simulate. Yet even these calculations scale only as a *fractional* power of the number of qubits. This allows us to simulate genuine multipartite Bell violations of GHZ states with 60 qubits, corresponding to a Hilbert space of a quintillion (10^{18}) dimensions.

Bell violations as large as this would also require a quintillion different measurement settings in the laboratory. At around 1 ms per measurement in an ion-trap experiment, full confirmation of a 60 qubit multipartite Bell violation would take over 30 million years, even with just one measurement per laboratory setting. For multipartite Bell inequalities, our simulations took less than 48 hours, so the exponential speedup obtained through phase space quantum simulations is a highly practical computational tool. To demonstrate applications for decoherence dynamics, we use the method to simulate the observed super-decoherence in ion traps.

The paper is organized as follows. In Section II we discuss the multipartite Bell inequalities. The sampling of the GHZ states using the positive P and the Q section are described in Sections III and IV, respectively. The computational results are shown in Section V. In Section VI we describe a decoherence model that shows the dynamical decay of the Bell inequality, as observed experimentally. Finally, Section VII gives a summary of

our results and conclusions.

II. MULTIPARTITE BELL INEQUALITIES

The challenge for quantum simulation is to simulate very large systems where quantum effects can still manifest themselves. The best example is a macroscopic superposition state of the type considered in the “Schrödinger cat” paradox. With this objective, we will analyze how to simulate the genuine multipartite Bell inequality violations of M entangled particles. Our goal is to determine whether this is possible, using probabilistic sampling. We also wish to understand the relevant scaling properties, as they depend on the measurements themselves. A detailed treatment of the bipartite case, including dynamical simulations, is presented elsewhere [22].

A. MABK Bell inequalities for M sites

First, we summarize well-known Bell inequalities that test local hidden variable (LHV) theories involving M spin-1/2 particles at different sites. We label the sites by j , where $j = 1, \dots, M$.

In the case of M particles emitted from a common source, measurements of M spatially separated observers are modeled in the LHV theory by taking random samples of a common set of parameters (the hidden variables) symbolized by λ . Measured values are then functions of some local detector/analyzer settings and the hidden parameters λ .

We use the notation that $X_m(\lambda) \equiv X_m(\theta_m, \lambda)$ for the m -th observer with the detector analyzer setting θ_m , denoting the measurement value by X_m . Here, the measurement event includes the selection of the measurement setting θ_m at each site. The M measurement events are assumed to be space-like separated. In an LHV theory the correlations are thus obtained from a probabilistic calculation of the form:

$$E(X_1, X_2, \dots, X_M) \equiv \left\langle \left[\prod_{m=1}^M X_m \right] \right\rangle = \int \left[\prod_{m=1}^M X_m(\lambda) \right] P(\lambda) d\lambda. \quad (2)$$

where $P(\lambda)$ is a probability distribution for the hidden variables λ .

One can consider that at each site the experimentalist makes one of two choices for the measurement. Here, we denote these two choices by the quantum observables \hat{x}_j and \hat{y}_j , and denote the outcomes associated with these measurements by X_j, Y_j respectively. Experimentally, one uses an adjustable polarizer or Rabi rotation at each site to determine which of the choices to make, and there are 2^M possible combinations. For each of these 2^M

choices, an ensemble of measurements is necessary to obtain the relevant correlations.

Following Mermin [27], we can construct for mathematical convenience the operator

$$\hat{A}_j = \hat{x}_j + i\hat{y}_j, \quad (3)$$

bearing in mind that this is not a measured observable. We can also define the complex function $F_j = X_j + iY_j$. We now examine the dichotomic case using qubits. We follow Mermin and choose:

$$\begin{aligned} \hat{x}_j &= \hat{\sigma}_j^{\theta_j} \\ \hat{y}_j &= \hat{\sigma}_j^{\theta_j + \pi/2}, \end{aligned} \quad (4)$$

where $\hat{\sigma}_j^\theta = \hat{\sigma}_j^x \cos \theta_j + \hat{\sigma}_j^y \sin \theta_j$, and $\hat{\sigma}_j^{x/y}$ are the Pauli spin operators. Therefore:

$$\hat{A}_j = (\hat{\sigma}_j^x + i\hat{\sigma}_j^y) e^{-i\theta_j}. \quad (5)$$

Next, we consider the measurable moments given by the expression:

$$A_{\text{QM}} = \langle \prod_{j=1}^M \hat{A}_j \rangle \equiv \langle \hat{A} \rangle, \quad \hat{A} \equiv \prod_{j=1}^M \hat{A}_j \quad (6)$$

and the corresponding LHV prediction for this moment

$$A_\lambda = \langle \prod_{j=1}^M \hat{A}_j \rangle_\lambda \equiv \langle \prod_{j=1}^M F_j \rangle.$$

where Π denotes the product (standard notation). One can expand the terms of the product, and write as a real and imaginary part: So, we define the real and imaginary parts by:

$$A_{\text{QM}/\lambda} = \text{Re} A_{\text{QM}/\lambda} + i \text{Im} A_{\text{QM}/\lambda}. \quad (7)$$

It is known that LHV theories place a constraint on what should be observed for these quantities. These are the Mermin-Ardehali-Belinskii-Klyshko (MABK) Bell inequalities. Mermin [27] originally derived the following Bell inequality (which we will call Mermin's inequality),

$$\text{Im} A_\lambda \leq \begin{cases} 2^{(M-1)/2}, & M \text{ is odd,} \\ 2^{M/2}, & M \text{ is even.} \end{cases} \quad (8)$$

The same inequalities hold for the $\text{Re} A_\lambda$. Mermin's inequality for even M is weak, and is not violated by the Bell state (12) for $M = 2$. Therefore for the case of even M we will follow Ardehali, Belinskii and Klyshko (ABK) [35–37], who derived the following inequalities:

$$\text{Re} A_\lambda + \text{Im} A_\lambda \leq \begin{cases} 2^{M/2}, & M \text{ is even,} \\ 2^{(M+1)/2}, & M \text{ is odd.} \end{cases} \quad (9)$$

ABK inequalities are stronger for even M , but not for odd M , and thus the MABK Bell inequalities [36, 37] are the combination of (8) for odd M , and (9) for even M .

We can expand these inequalities explicitly to see what they are. For $M = 2$, $\theta_j = 0$, the MABK inequality is:

$$\langle \sigma_1^x \sigma_2^y \rangle_\lambda + \langle \sigma_1^y \sigma_2^x \rangle_\lambda + \langle \sigma_1^x \sigma_2^x \rangle_\lambda - \langle \sigma_1^y \sigma_2^y \rangle_\lambda \leq \sqrt{2} \quad (10)$$

which is the famous Clauser-Horne-Shimony-Holt (CHSH) Bell inequality. For $M = 3$, $\theta_j = 0$ the resulting inequality is:

$$\langle \sigma_1^y \sigma_2^x \sigma_3^x \rangle_\lambda + \langle \sigma_1^x \sigma_2^y \sigma_3^x \rangle_\lambda + \langle \sigma_1^x \sigma_2^x \sigma_3^y \rangle_\lambda - \langle \sigma_1^y \sigma_2^y \sigma_3^y \rangle_\lambda \leq 2 \quad (11)$$

as derived by Mermin. We note by defining $F_j = X_j - iY_j$ a different set of MABK inequalities with different signs can be derived.

B. MABK violations with a GHZ state

All of the MABK inequalities are predicted by LHV theories, but only for the right quantum state are they maximally violated. Let us consider the GHZ state:

$$|\psi\rangle = \frac{1}{\sqrt{2}} \left(\bigotimes_{j=1}^M |\uparrow\rangle_j + e^{i\phi} \bigotimes_{j=1}^M |\downarrow\rangle_j \right), \quad (12)$$

where $|\uparrow\rangle_j$ $|\downarrow\rangle_j$ are the eigenstates of $\hat{\sigma}_j^z$. It is known that the state (12) with $r = M$ violates (9) by the *maximum* amount predictable by Quantum Mechanics (QM) [45]. For the Mermin-type inequalities (8), this maximal violation occurs for the angle $\phi = \pi/2$ and the measurement choice $\theta_j = 0$:

$$A_j = \sigma_j^x + i\sigma_j^y, \quad j = 1, \dots, M. \quad (13)$$

where we have now denoted the results X_j , Y_j of the measurements $\hat{\sigma}_j^x$, $\hat{\sigma}_j^y$ by σ_j^x , σ_j^y written without the operators. This orthogonal angle choice corresponds to the famous cases of the EPR-Bohm and GHZ paradoxes [23, 46, 47], that yield perfect correlations between spatially separated spins. The quantum prediction for the choice of measurement orientations (13) is [27]:

$$\text{Im} A_{\text{QM}} = 2^{M-1}. \quad (14)$$

On the other hand, the Ardehali-Bell-CHSH-type inequalities (9) give a maximum when $\phi = \pi$ and one site has a shifted measurement angle:

$$\begin{aligned} F_j &= \sigma_j^x - i\sigma_j^y, \quad j \neq M \\ F_M &= \sigma^{-\pi/4} + i\sigma^{\pi/4}. \end{aligned} \quad (15)$$

We note this corresponds for $M = 2$ to the case of Bell and CHSH [48–51]. Here, the measurement choice does not allow perfect correlation between spatially separated measurements for a fixed setting, and the violation is

obtained statistically. The quantum prediction in this case is [27, 35]:

$$\text{Re}A_{\text{QM}} + \text{Im}A_{\text{QM}} = 2^{M-1/2}. \quad (16)$$

It is convenient to join the odd- and even- M inequalities using an operator

$$\hat{V} = \begin{cases} \text{Re}\hat{A} + \text{Im}\hat{A}, & M \text{ is even,} \\ \sqrt{2}\text{Im}\hat{A}, & M \text{ is odd.} \end{cases} \quad (17)$$

In this case the MABK inequality for all M is, in the case of an LHV theory:

$$V_\lambda \equiv |\langle \hat{V} \rangle_\lambda| \leq 2^{M/2}. \quad (18)$$

This is violated by quantum mechanics with the state and measurement choices above, since:

$$V_{\text{QM}} \equiv \langle \hat{V} \rangle = 2^{M-1/2} > V_\lambda. \quad (19)$$

The ratio between the LHV limit and the QM result is thus:

$$\frac{V_{\text{QM}}}{V_\lambda} \geq 2^{(M-1)/2}, \quad (20)$$

which grows exponentially with M .

C. Genuine M -partite Bell nonlocality

Svetlichny [38] introduced the idea of genuine multipartite nonlocality. He derived inequalities that if violated indicate a three-body (rather than two-body) nonlocality. The inequalities have been generalized to M -partite cases by Collins *et al* [39] and by Seevinck and Svetlichny [52]. We point out that other recent works [53–55] have improved Svetlichny's approach further.

The Svetlichny-CGPRS inequality is:

$$V_S \equiv \text{Re}A_\lambda + \text{Im}A_\lambda \leq 2^{M-1}, \quad (21)$$

the violation of which is sufficient to confirm *genuine M -partite Bell nonlocality*. For $M = 3$ this means that the violation cannot be explained using product states or mixtures with Bell nonlocality between only two sites. More generally, for arbitrary M , this terminology means that the violation cannot be explained using states with a genuine m -partite Bell nonlocality, where $m < M$. The quantum prediction maximizes at (16) to predict violation, for even M , by a *constant* amount:

$$\frac{V_{\text{QM}}}{V_S} = \sqrt{2}. \quad (22)$$

This constant violation ratio differs from the exponential violation predicted for the MABK inequalities, which makes the effect both harder to measure experimentally, and more difficult to simulate than the usual Bell inequality. However it is necessary to achieve this stronger correlation if one wishes to assert that a given superposition is truly macroscopic to a given level, i.e., if one wishes to exclude the possibility that there are only microscopic violations of local realism present in a quantum system.

III. SAMPLING GHZ STATES WITH POSITIVE PHASE-SPACE DISTRIBUTIONS

The states we wish to sample are GHZ states (12), which are experimentally prepared in a number of photonic and ion-trap experiments. We rewrite these as:

$$|\Phi\rangle = \frac{1}{\sqrt{2}} (|\uparrow \dots \uparrow\rangle + e^{i\phi} |\downarrow \dots \downarrow\rangle). \quad (23)$$

Of course, any experiment will inevitably also include other states owing to decoherence effects. Here we wish to start by considering the pure state, which is a worst-case scenario from the point of view of phase-space simulations. The up- and down-states can be represented differently, depending on the underlying physical system, which will in turn affect the sampling. We will consider different sampling techniques using different operator representations, in order to compare their efficiency.

A. Phase-space methods

In general terms, a phase-space representation is a mapping from a c-number distribution function $P(\vec{\lambda})$ to a density matrix $\hat{\rho}$, defined by

$$\hat{\rho} = \int P(\vec{\lambda}) \hat{\Lambda}(\vec{\lambda}) d\vec{\lambda}. \quad (24)$$

Here $\hat{\Lambda}(\vec{\lambda})$ is a complete operator basis, which is parametrized with a phase-space variable $\vec{\lambda}$, and $P(\vec{\lambda})$ is a distribution over $\vec{\lambda}$ which typically allows one to calculate observables as moments. For our present purposes, we will focus on mappings that involve a positive-definite distribution $P(\vec{\lambda})$. This allows probabilistic sampling, which is a very scalable route for calculating high-dimensional integrals and correlations. It also removes the need to have a numerical representation of an exponentially large matrix. This approach results in efficient scaling for low-order correlations, even for highly nonclassical states like the GHZ state, and can be sampled for high-order correlations with somewhat lower efficiency.

There are many such mappings known. The earliest methods developed were for the Wigner function [56], Q-function [31] and P-function [57, 58]. These are all for bosonic Hilbert spaces, are defined for a real phase-space $\vec{\lambda}$, and correspond to different operator orderings. Of these, only the Q-function is positive-definite. Subsequently, positive-definite extensions of these were developed that use complex instead of real phase-spaces, including the positive P-representation [16], the positive Wigner representation [59, 60] and the Gaussian representation [61]. The positive P-representation is useful, as it combines stochastic time-evolution with simple observables.

All these bosonic methods involve a Hilbert space of too large a dimension for optimum sampling of the GHZ state, as we explain below. It is most efficient to only represent those parts of a Hilbert space that are measured. Hence, it is better to use a phase-space representations that is specifically matched to a finite dimensional Hilbert space. The earliest of these were the SU(2) based continuous representations [32, 62, 63], which employ Lie group methods. These have a similar form to the bosonic case. Once again, there are both positive and non-positive distributions, as well as complex phase-space methods [64]. A widely used positive form is the SU(2) Q-function [32, 33], which we analyze in detail in the next section.

Recently, a number of interesting and innovative methods have been introduced that treat finite Hilbert spaces in a different way. These replace the integral in Eq (24) with a summation over a finite set of points. Using this technique, it is possible to develop a discrete Wigner distribution [65–70], which uses hermitian matrices instead of distributions to represent the Hilbert space. In the standard construction of such methods, certain specific quantum states have positive representations, but this is not true in general. In other words, the generic case for the discrete Wigner distribution is that the mapping is non-positive.

These discrete approaches have the property that the underlying discrete Wigner distribution is a $2^M \times 2^M$ matrix for M qubits [67, 68, 70]. In the largest case treated here, with $M = 60$, this involves 10^{36} matrix elements. These do not all have to be stored in memory, which is impossible with current computers. Nevertheless, calculating observables with 10^{36} elements requires sampling to reduce the computation time. As the elements are not all positive, this would presumably involve a sign or phase term, which can lead to inefficiencies.

Accordingly, we do not investigate the discrete Wigner function here. Yet such methods may also be useful. The main challenge is that the resulting large matrix representations are not probabilistic. The question of how to sample these efficiently is an open question at present. However, extending such discrete techniques to allow probabilistic sampling may not be impossible. This is outside the scope of the present paper, so we now return to the question of efficient sampling using continuous, positive

phase-space distributions.

B. Positive P-representation

We first consider the positive P-representation [16]. This is a probabilistic phase-space representation widely used in quantum optics. It is most suitable when using photonic methods to obtain qubit observables, as it can represent any multi-mode bosonic quantum state. With this representation, a general quantum density matrix $\hat{\rho}$ is represented using a positive distribution $P(\vec{\alpha}, \vec{\beta})$, where:

$$\hat{\rho} = \int P(\vec{\alpha}, \vec{\beta}) \hat{\Lambda}(\vec{\alpha}, \vec{\beta}) d^{2M} \vec{\alpha} d^{2M} \vec{\beta}. \quad (25)$$

Here the projector $\hat{\Lambda}$ is:

$$\hat{\Lambda}(\vec{\alpha}, \vec{\beta}) = \frac{|\vec{\alpha}\rangle \langle \vec{\beta}^*|}{\langle \vec{\beta}^* | \vec{\alpha} \rangle}, \quad (26)$$

where $|\vec{\alpha}\rangle = |\alpha_1 \dots \alpha_n\rangle$ is a multi-mode coherent state.

This representation maps quantum states into $4M$ real coordinates: $\vec{\alpha}, \vec{\beta}$, which is twice the dimension of a classical phase-space. The expectation of any normally ordered observable $\hat{O} \equiv O(\hat{a}_1^\dagger, \hat{a}_1, \dots)$ is then:

$$\langle \hat{O} \rangle = \int O(\beta_1, \alpha_1, \dots) P(\vec{\alpha}, \vec{\beta}) d^{2M} \vec{\alpha} d^{2M} \vec{\beta}. \quad (27)$$

A general, although non-unique positive construction is:

$$P(\vec{\alpha}, \vec{\beta}) = \frac{\langle \vec{\mu} | \hat{\rho} | \vec{\mu} \rangle}{(2\pi)^{2M}} e^{-|\vec{\nu}|^2}, \quad (28)$$

where we have made a variable change to sum and difference variables:

$$\vec{\nu} = (\vec{\alpha} - \vec{\beta}^*)/2, \quad \vec{\mu} = (\vec{\alpha} + \vec{\beta}^*)/2. \quad (29)$$

C. Spin state representation

The natural choice for up- and down-states are spin states $|\uparrow\rangle \equiv |10\rangle$, $|\downarrow\rangle \equiv |01\rangle$. Spin operators can be mapped into bosons with the Schwinger representation [71]:

$$\begin{aligned} \sigma_j^x &= \hat{a}_j'^\dagger \hat{a}_j'' + \hat{a}_j''^\dagger \hat{a}_j', \\ \sigma_j^y &= \frac{1}{i} (\hat{a}_j'^\dagger \hat{a}_j'' - \hat{a}_j''^\dagger \hat{a}_j'), \\ \sigma_j^z &= \hat{a}_j'^\dagger \hat{a}_j' - \hat{a}_j''^\dagger \hat{a}_j'', \end{aligned} \quad (30)$$

where $\hat{a}_j'^\dagger$ creates a particle in the first position of the j -th spin operator, and $\hat{a}_j''^\dagger$ creates one in the second

position. Substituting $\hat{\rho} = |\Phi\rangle\langle\Phi|$ into (28) and performing the substitution (29), we get the following positive-P function:

$$P = \frac{1}{2\pi^{4M}} e^{-|\vec{\nu}|^2} e^{-|\vec{\mu}'|^2 - |\vec{\mu}''|^2} \left| \prod_{j=1}^M \mu'_j + e^{-i\phi} \prod_{j=1}^M \mu''_j \right|^2. \quad (31)$$

To sample this distribution, we use the von Neumann rejection method, which requires a known reference distribution as an upper bound. This distribution is bounded above by the following expression:

$$P \leq 2G(\vec{\nu})P_0(\vec{\mu}), \quad (32)$$

where:

$$G(\vec{\nu}) = \frac{1}{\pi^{2M}} e^{-|\vec{\nu}|^2}, \quad (33)$$

and

$$P_0 = \frac{1}{2\pi^{2M}} e^{-|\vec{\mu}'|^2 - |\vec{\mu}''|^2} \left(\prod_{j=1}^M |\mu'_j|^2 + \prod_{j=1}^M |\mu''_j|^2 \right). \quad (34)$$

These two reference distributions can be sampled exactly using a combination of Gamma and Gaussian variates. The expectation of the Mermin operator \hat{A} of interest here is then given by:

$$\langle \hat{A} \rangle = \int d^{4M} \vec{\alpha} d^{4M} \vec{\beta} P(\vec{\mu}(\vec{\alpha}, \vec{\beta}), \vec{\nu}(\vec{\alpha}, \vec{\beta})) \times \prod_{j=1}^M ((\beta'_j \alpha''_j + i s_j \beta''_j \alpha'_j) e^{-i s_j \theta_j}). \quad (35)$$

While this method is able to sample the required GHZ state, the sampling is rather inefficient. We can improve the results using a more compact Hilbert space mapping technique, described in the next subsection.

D. Number state representation

Sampling is generally improved if the Hilbert space dimension is reduced as far as possible, to eliminate samples that overlap the unused part of the space. We can decrease the number of dimensions in the required phase space by half, by using number states instead of spin states. This is possible because we really only need the fact that occupations are binary.

This can be done because our operators of interest — \hat{A} — depend on σ_x^j and σ_y^j linearly. Therefore if we denote $|\uparrow\rangle \equiv |1\rangle$, $|\downarrow\rangle \equiv |0\rangle$, we can formally write:

$$\begin{aligned} \sigma_x^j &= \hat{a}_j + \hat{a}_j^\dagger, \\ \sigma_y^j &= \frac{1}{i} (\hat{a}_j^\dagger - \hat{a}_j), \\ \sigma_z^j &= \hat{a}_j - \hat{a}_j^\dagger. \end{aligned} \quad (36)$$

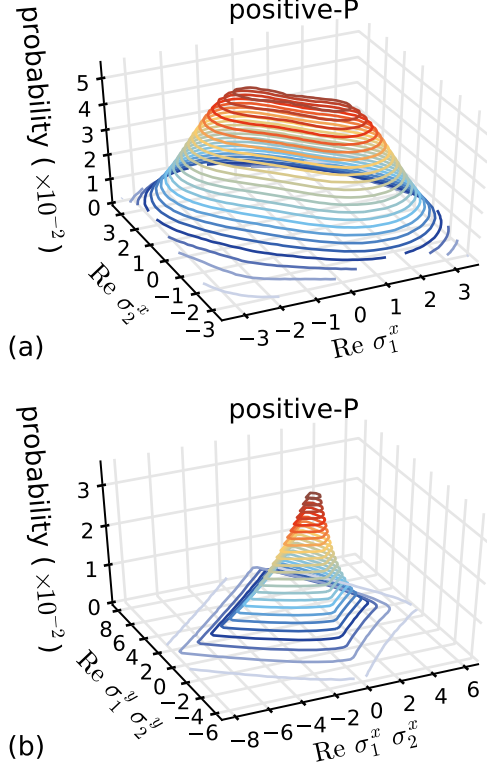


Figure 1. Correlations for the different parts of the quantity (43) in the positive-P representation, with the number state method and 2^{26} samples.

One can verify that, for instance, $|0\rangle + |1\rangle$ is an eigenstate of σ_x :

$$\langle \Phi | \sigma_x (|0\rangle + |1\rangle) = \langle \Phi | (|0\rangle + |1\rangle + |2\rangle) = \langle \Phi | (|0\rangle + |1\rangle). \quad (37)$$

Just as in the previous subsection, substituting $\hat{\rho} = |\Phi\rangle\langle\Phi|$ into (28) and performing the substitution (29), we get the positive-P function:

$$\begin{aligned} P &= \frac{1}{2\pi^{2M}} e^{-|\vec{\nu}|^2} e^{-|\vec{\mu}|^2} \\ &\times \left(1 + \prod_{j=1}^M \mu_j^* \mu_j + e^{-i\phi} \prod_{j=1}^M \mu_j^* + e^{i\phi} \prod_{j=1}^M \mu_j \right) \\ &= \frac{1}{2\pi^{2M}} e^{-|\vec{\nu}|^2} e^{-|\vec{\mu}|^2} \left| \prod_{j=1}^M \mu_j + e^{-i\phi} \right|^2. \end{aligned} \quad (38)$$

The target distribution can be sampled using von Neumann rejection sampling:

$$P \leq 2G(\vec{\nu})P_0(\vec{\mu}), \quad (39)$$

where the reference distributions are now:

$$G(\vec{\nu}) = \frac{1}{\pi^{2M}} e^{-|\vec{\nu}|^2}, \quad (40)$$

$$P_0 = \frac{1}{2\pi^M} e^{-|\vec{\mu}|^2} \left(\left| \prod_{j=1}^M \mu_j \right|^2 + 1 \right). \quad (41)$$

In this representation the expectation of the target operator is:

$$\begin{aligned} \langle \hat{A} \rangle &= \int d^{2M} \vec{\alpha} d^{2M} \vec{\beta} P \left(\vec{\mu}(\vec{\alpha}, \vec{\beta}), \vec{\nu}(\vec{\alpha}, \vec{\beta}) \right) \\ &\times \prod_{j=1}^M ((\alpha_j + i s_j \beta_j) e^{-i s_j \theta_j}). \end{aligned} \quad (42)$$

In Figure (1), we show the distribution of results with the positive-P representations, for a portion of the Ardehali inequality for the case $M = 2$, given by:

$$F_{XY} = -\langle \hat{\sigma}_1^x \hat{\sigma}_2^x \rangle + \langle \hat{\sigma}_1^y \hat{\sigma}_2^y \rangle. \quad (43)$$

In a LHV theory the values of $\text{Re } \sigma_x^1$ and $\text{Re } \sigma_x^2$ are limited to the range $[-1, 1]$, but clearly our results are not limited to that range. This essential feature means that Bell's theorem does not limit our results, because the sampled values are not the same as their physical eigenvalues [72]. The connection with weak values [28] has been discussed in a previous paper [22]. This demonstrates an essential feature of this phase-space representation: it is analogous to a weak-value measurement, giving results outside the normal range of the eigenvalues.

We note that this is still a positive phase-space representation, valid in a more limited subspace than before, but certainly able to represent the GHZ state. However, both approaches have the drawback that they use methods designed to represent infinite dimensional Hilbert spaces, which is not a good match to the GHZ state requirements.

IV. SAMPLING GHZ STATES WITH THE Q-FUNCTION

The Hilbert space occupied by the GHZ state is a finite-dimensional Hilbert space for which such an infinite-dimensional bosonic mapping is not strictly necessary. Next we turn to methods that are more suited to the task of representing finite dimensional states. Our interest in doing this is to determine if this can improve the sampling properties.

The Q-function for bosons was first introduced by Husimi [31] as an expectation value of the density matrix in an over-complete coherent-state basis. It gives a mapping of a general many-body density matrix into a unique, positive distribution. This method has been widely used as a method to probabilistically represent statistical properties in quantum optics. It has had a diverse range of applications, mostly in tomography.

The same technique can be used to define a multipartite Q-function based on SU(2) coherent states, as an

alternative and more efficient means of phase-space sampling for qubits.

A. The SU(2) Q-function

For purposes of calculations, we will consider as the basis set an un-normalized version of the SU(2) coherent states [32, 62, 63] defined as:

$$|\vec{z}\rangle = \prod_{j=1}^M \left(|0\rangle_j + z_j |1\rangle_j \right). \quad (44)$$

In terms of this un-normalized state the resolution of unity is given by:

$$\int d^2 \vec{z} \left(\prod_{j=1}^M \mathcal{N}(|z_j|^2) \right) |\vec{z}\rangle \langle \vec{z}| = \hat{1}. \quad (45)$$

Here we have defined the normalization factor $\mathcal{N}(|z_j|^2)$ as:

$$\mathcal{N}(|z_j|^2) = \frac{2}{\pi} \frac{1}{(1 + |z_j|^2)^3}. \quad (46)$$

Using the resolution of unity for the un-normalized SU(2) coherent states (45), we can define a Q-function:

$$Q(\vec{z}) = \left[\prod_{j=1}^M \mathcal{N}(|z_j|^2) \right] \langle \vec{z} | \hat{\rho} | \vec{z} \rangle, \quad (47)$$

which has the property that:

$$\int d^2 \vec{z} Q(\vec{z}) = 1. \quad (48)$$

This Q-function is positive definite and is defined for any quantum density matrix and is normalized to one.

In our GHZ state of interest (23) we denote $|\downarrow\rangle = |0\rangle$ and $|\uparrow\rangle = |1\rangle$. Hence for the density matrix $\hat{\rho} = |\Phi\rangle\langle\Phi|$ we obtain:

$$\begin{aligned} \langle \vec{z} | \hat{\rho} | \vec{z} \rangle &= \langle \vec{z} | |\Phi\rangle\langle\Phi| | \vec{z} \rangle = |\langle \vec{z} | |\Phi\rangle|^2 \\ &= \frac{1}{2} \left| \prod_j (j \langle 0 | + z_j^* \langle 1 |) (|1 \dots 1\rangle + e^{i\phi} |0 \dots 0\rangle) \right|^2 \\ &= \frac{1}{2} \left| \prod_j z_j + e^{-i\phi} \right|^2. \end{aligned} \quad (49)$$

Therefore the Q-function for our states of interest is:

$$Q(\vec{z}) = \frac{1}{2} \left(\frac{2}{\pi} \right)^M \prod_{j=1}^M \frac{1}{(1 + |z_j|^2)^3} \left| \prod_j z_j + e^{-i\phi} \right|^2 \quad (50)$$

The expectation value of \hat{A} can be expressed in terms of the Q-function using (59), the details of the evaluations are shown in the next section, and the fact that $\sigma_x^j = 2\hat{S}_x^j = \hat{S}_+^j + \hat{S}_-^j$ and $\sigma_y^j = 2\hat{S}_y^j = (\hat{S}_+^j - \hat{S}_-^j)/i$, hence:

$$\hat{A} = \prod_{j=1}^M \left(((1+s_j)\hat{S}_+^j + (1-s_j)\hat{S}_-^j) e^{-is_j\theta_j} \right). \quad (51)$$

Therefore the expectation value of the target operator using the Q-function is:

$$\begin{aligned} \langle \hat{A} \rangle &= \langle \Phi | \hat{A} | \Phi \rangle \\ &= \int d\vec{z} Q(\vec{z}) \frac{3^M}{\prod_j (1+|z_j|^2)} \\ &\quad \times \prod_{j=1}^M ((1+s_j)z_j^* + (1-s_j)z_j) e^{-is_j\theta_j}. \end{aligned} \quad (52)$$

B. Evaluation of moments

In this section we show the evaluation of the moments of the form $\langle \prod_j \hat{S}_{d_j}^j \rangle$ with directions $d_j \in \{-, +\}$, in terms of the SU(2) Q-function. In order to evaluate the moments, we notice that we can express the action of the raising spin operators on the un-normalized SU(2) coherent state $|\mathbf{z}\rangle$ as a derivative of the SU(2) coherent state $|\vec{z}\rangle$, so that:

$$\begin{aligned} \hat{S}_+^j |\vec{z}\rangle &= \hat{S}_+^j \left(\prod_j e^{\hat{S}_+^j z_j} |0\rangle_j \right) \\ &= \frac{\partial}{\partial z_j^*} \left(\prod_j e^{\hat{S}_+^j z_j} |0\rangle_j \right) \\ &= \frac{\partial}{\partial z_j^*} |\vec{z}\rangle. \end{aligned} \quad (53)$$

Similarly, there is a conjugate expression:

$$\begin{aligned} \langle \vec{z} | \hat{S}_-^j &= \langle 0 | e^{\hat{S}_-^j \vec{z}} \hat{S}_-^j \\ &= \frac{\partial}{\partial z_j^*} \left(\prod_j \langle 0 | e^{\hat{S}_-^j \vec{z}} \right) \\ &= \frac{\partial}{\partial z_j^*} \langle \vec{z} |, \end{aligned} \quad (54)$$

while for the z -direction one obtains:

$$\begin{aligned} \hat{S}_z^j |\mathbf{z}\rangle &= \hat{S}_z^j \left(\prod_j e^{\hat{S}_+^j z_j} |0\rangle_j \right) \\ &= \prod_j \frac{1}{2} (-|0\rangle_j + z_j |1\rangle_j) \\ &= \prod_j \frac{1}{2} \left(2z_j \frac{\partial}{\partial z_j} - 1 \right) |\mathbf{z}\rangle. \end{aligned} \quad (55)$$

Here we have used that:

$$z_j \frac{\partial}{\partial z_j} (|0\rangle_j + z_j |1\rangle_j) = z_j |1\rangle_j, \quad (56)$$

and hence the last identity above is obtained from:

$$2z_j \frac{\partial}{\partial z_j} \|\mathbf{z}\rangle - \|\mathbf{z}\rangle = z_j |1\rangle_j - |0\rangle_j. \quad (57)$$

Next, we evaluate the moments of the spin operators \hat{S}_+^j , \hat{S}_-^j and \hat{S}_z^j using the resolution of unity (45) as well as the definition of the Q-function (47) so that:

$$\begin{aligned} \left\langle \prod_j \hat{S}_{d_j}^j \right\rangle &= \text{Tr} \left[\hat{\rho} \prod_j \hat{S}_{d_j}^j \right] \\ &= \int d^2 \vec{z} \prod_j \mathcal{N}(|z_j|^2) \\ &\quad \times \left(\prod_{d_j=-} \frac{\partial}{\partial z_j^*} \right) \langle \vec{z} | \hat{\rho} \left(\prod_{d_j=+} \frac{\partial}{\partial z_j} \right) |\vec{z}\rangle \end{aligned} \quad (58)$$

Integrating by parts for each j , providing that the boundary terms vanish, we get:

$$\begin{aligned} \left\langle \prod_j \hat{S}_{d_j}^j \right\rangle &= (-1)^M \int d^2 \vec{z} \langle \vec{z} | \hat{\rho} |\vec{z}\rangle \\ &\quad \times \prod_{j,d_j=-} \frac{\partial \mathcal{N}(|z_j|^2)}{\partial z_j^*} \prod_{j,d_j=+} \frac{\partial \mathcal{N}(|z_j|^2)}{\partial z_j} \\ &= \int d^2 \vec{z} Q(\vec{z}) \frac{3^M}{\prod_j (1+|z_j|^2)} \prod_{j,d_j=-} z_j \prod_{j,d_j=+} z_j^*. \end{aligned} \quad (59)$$

Here we have used that the derivative of $\mathcal{N}(|z_j|^2)$ is:

$$\begin{aligned} \frac{1}{\mathcal{N}(|z_j|^2)} \frac{\partial}{\partial z_j^*} \mathcal{N}(|z_j|^2) &= \frac{2}{\pi \mathcal{N}(|z_j|^2)} \frac{\partial}{\partial z_j^*} \frac{1}{(1+|z_j|^2)^3} \\ &= \frac{-3z_j^*}{(1+|z_j|^2)}. \end{aligned} \quad (60)$$

Here, the results of Q-function sampling of the GHZ state are presented. Firstly we show the results of the difference between the calculations with the positive-P and SU(2)-Q representations, using a portion of the Ardehali inequality for the case $M = 2$, given as previously by:

$$F_{XY} = -\langle \hat{\sigma}_1^x \hat{\sigma}_2^x \rangle + \langle \hat{\sigma}_1^y \hat{\sigma}_2^y \rangle. \quad (61)$$

In Fig. 2(a) we show the correlation between the real parts of $\hat{\sigma}_i^x$, $i = 1, 2$ of the quantity F_{XY} , while the correlation between the two terms of (61) is plotted in Fig. 2(b). Once again, this method is analogous to a weak-value measurement, giving results outside the normal range of the eigenvalues.

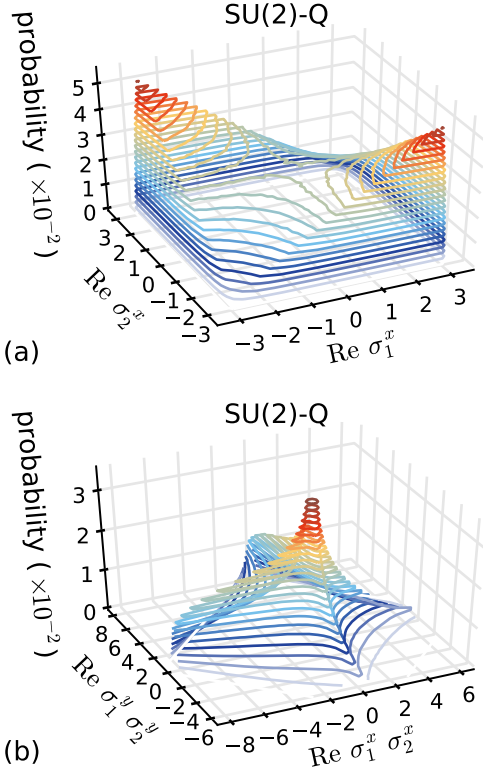


Figure 2. Correlations for the different parts of the quantity (61) in the SU(2)-Q representation, 2^{26} samples.

For the spin operator \hat{S}_z^j we obtain:

$$\begin{aligned} \left\langle \prod_j \hat{S}_z^j \right\rangle &= \text{Tr} \left[\prod_j \hat{\rho} \hat{S}_z^j \right] \\ &= \prod_j \int d^2 z_j \mathcal{N}(|z_j|^2) \langle \mathbf{z} | \hat{\rho} \left(z_j \frac{\partial}{\partial z_j} - \frac{1}{2} \right) | \mathbf{z} \rangle. \end{aligned} \quad (62)$$

Next we use the following result, which also involves partial integration:

$$\begin{aligned} &\prod_j \int d^2 z_j \mathcal{N}(|z_j|^2) \langle \mathbf{z} | \hat{\rho} z_j \frac{\partial}{\partial z_j} | \mathbf{z} \rangle \\ &= - \prod_j \int d^2 z_j \langle \mathbf{z} | \hat{\rho} | \mathbf{z} \rangle \frac{\partial}{\partial z_j} \left(z_j \mathcal{N}(|z_j|^2) \right) \\ &= \prod_j \int d^2 z_j Q(\mathbf{z}) \left(\frac{3|z_j|^2}{(1+|z_j|^2)} - 1 \right), \end{aligned} \quad (63)$$

and leads to our final spin operator identity,

$$\left\langle \prod_j \hat{S}_z^j \right\rangle = \prod_j \frac{3}{2} \int d^2 z_j Q(\mathbf{z}) \left(\frac{|z_j|^2 - 1}{|z_j|^2 + 1} \right). \quad (64)$$

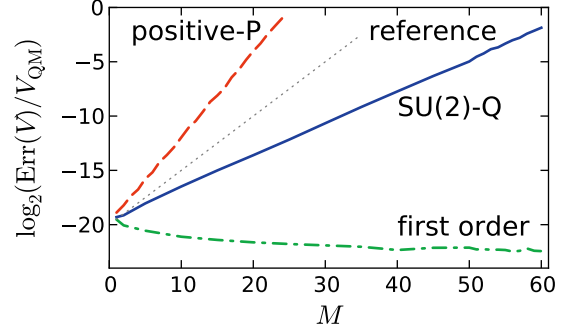


Figure 3. Scaling properties for sampled correlations of multiparticle GHZ states. Relative errors are plotted for high order (V) correlations, (blue line) and first order correlations, or total number of “spin-ups” (green dashed line) using the SU(2)-Q representation with 2^{40} samples. The dotted reference line shows the point at which the sampling errors would give scaling properties of an experimental measurement. The red dotted line shows the scaling of the V correlations using the less efficient positive-P representation.

V. MULTIPARTITE BELL VIOLATION RESULTS

To simulate multipartite Bell violations, the GHZ state (23) was sampled using probabilistic random number generators using both Q-function and positive P-distribution methods. Of the two positive P-distribution mappings, the Schwinger representation method is less compact, and has a larger sampling error. For the results graphed here, we therefore chose the number state positive-P distribution. Although more efficient than the Schwinger representation, this still has a large basis set that corresponds to an infinite dimensional Hilbert space, with a much larger dimension than is needed for the GHZ state.

The lowest sampling errors were obtained with the SU(2) Q-distribution method, which uses a much more compact Hilbert space, having a dimension equal to the physical qubit dimension.

A. Multipartite sampling error properties

We initially investigate the scaling properties of the sampling errors as the number of qubits M is varied. This also determines the time taken for the simulation to reach a predetermined error, since one can include more parallel samples to reduce the simulated errors to any desired level.

First we consider the scaling with system-size of the sampling errors for *single* measurements of a low-order spin correlation (Fig. 3). For low-order correlation we have chosen the total number of “spin-ups” $N = \langle \sum_{j=1}^M (\hat{\sigma}_z^j + 1) / 2 \rangle$. In this case we noticed that the sampling errors *decreases* as M increases.

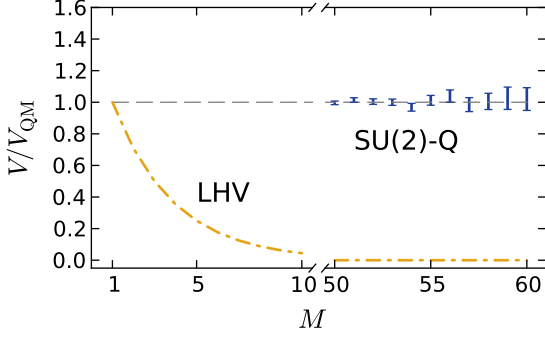


Figure 4. Violations for multi-particle GHZ states. Simulated Mermin violation using $SU(2)$ -Q representation with 2^{43} samples. The values of expectations and errors are normalized by the quantum mechanical prediction for the corresponding M . The horizontal grey dashed line gives the quantum prediction. The error bars show the sampled result and estimated sampling errors at each value of M . The dash-dotted line is the LHV prediction, which gives a Bell violation when above this line. Genuine multipartite Bell violations occur for even M when $V/V_{QM} > 1/\sqrt{2}$.

In contrast to this, high-order correlations showed exponentially increasing sampling error. The relative error in V scales as $2^{M/3}$, meaning that the time taken at constant error scales as $2^{2M/3}$. This means that probabilistic sampling scales more favorably than experiment, which would take time in proportion to 2^M . Therefore, the sampling takes place in times that scale $2^{M/3}$ times faster than any possible experiment.

In practical terms, such laboratory measurements would be highly nontrivial, due to the need to eliminate background noise for high-order correlations. No correlation measurements of this size have been reported to date. Experimentally, it is possible that such high-order correlations will be reported in future.

Even then, it is likely that one may only be able to measure a subset of all the high-order correlations possible for large M values. This is because of the enormous time required to make all possible correlation measurements for these inequalities, which is exponentially slower than the phase-space simulation.

B. Simulations of multipartite genuine Bell violations

In Fig. 4 we show the expectation value of the multipartite, multi-measurement quantity V compared with the quantum mechanical prediction $\langle V \rangle_{QM}$ from sampling the $SU(2)$ Q-distribution. The dashed line is the minimum correlation required to demonstrate a Bell violation, with a number of qubits ranging from $M = 2$ to $M = 60$. For all cases we verified clear Bell violations to at least 12 standard deviations from the classical limit.

Genuine multipartite violations of LHV, requiring all

M observers to participate, were verified for even M to at least 4 standard deviations. These cases all satisfied the more stringent requirement that:

$$V/V_{QM} > 1/\sqrt{2}. \quad (65)$$

The simulations were carried out using graphical processor unit (GPU) technology at a clock speed of 1.2 GHz, which allowed calculations with 50 GPUs on 22,000 parallel computational cores. The plotted results correspond in the 60 qubit case to simulating the results of a quintillion (10^{18}) distinct sixtieth order correlation functions. This took less than 48 hours. A reasonable estimate of the laboratory time-scale for carrying out all possible correlation measurements, at $10^{-3}s$ per measurement setting, is 3×10^7 years. This is more than 10^9 times slower than the simulations.

VI. DECOHERENCE SIMULATIONS

We have shown that it is possible to simulate genuine Bell violations, as well as obtaining scaling laws for GHZ states using phase space methods. But we can also ask whether it is also possible to use the positive phase-space methods to simulate decoherence processes? In order to answer this question, here we will focus on the question of the study of dynamical noise and decoherence in ion traps, which is an important issue in the observation of mesoscopic quantum effects [73]. Ion traps have been widely used in order to create entangled states and also to investigate the decay rate of GHZ states [74].

Here we will follow the noise model of Monz et al. [74], which was used to explain the observed super-decoherence found in ion-trap experiments. This is physically due to the fact that the magnetic field noise reservoir is correlated over all the qubits. As a result, they do not decohere with independent noise or error sources, as is often assumed theoretically. To model this, we assume a delta-correlated magnetic field noise which is shared by all the ions, such that

$$\langle \Delta B(t) \Delta B(t') \rangle = \Delta B_0^2 \delta(t - t'). \quad (66)$$

In this case we assume that the interaction or noise Hamiltonian is:

$$\hat{H} = \frac{\mu \Delta B(t)}{2} \sum_{j=1}^M \hat{\sigma}_z^j. \quad (67)$$

This model can be simulated dynamically multiplying, in each of the samples after every time step Δt , an independent noise term $\exp(i\epsilon N \zeta_j)$ by the value corresponding to the operator $\prod_{j=1}^M (\hat{\sigma}_x^j + \hat{\sigma}_y^j)$. We use the respectively measurement choice V of (17) for odd M and even M . Here

$$\epsilon = \mu \Delta B_0 \sqrt{\Delta t} / \hbar \quad (68)$$

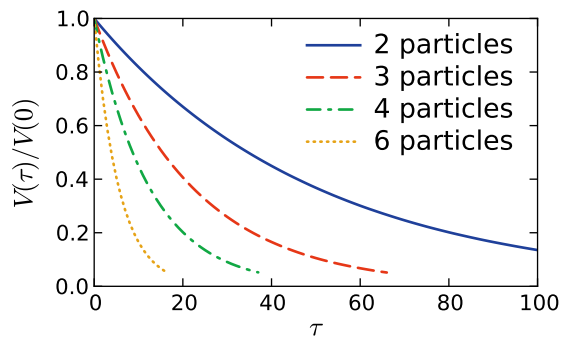


Figure 5. Decay of the sampled quantity V using the model of super-decoherence of Eq (67), for 2 (solid blue line), 3 (red dashed line), 4 (green dash-dotted line) and 6 (yellow dotted line) particles, with decoherence rate $\epsilon = 0.1$. The horizontal axis is the dimensionless time, $\tau = t/\Delta t$.

defines the speed of the decoherence, and ζ_j is a Gaussian random number such that

$$\langle \zeta_j \zeta_{j'} \rangle = \delta_{jj'}. \quad (69)$$

The results of the simulation are shown in Fig. 5. This demonstrates the experimentally observed quadratic decoherence, with decay times scaling with $1/M^2$ as M increases over a range comparable to current experiments, therefore showing the effect of super-decoherence.

VII. CONCLUSIONS

Our main result is that it is possible to sample quantum events probabilistically, even when they display macroscopic quantum paradoxes and Schrödinger cat behavior. This is not prohibited by the Bell inequality, although we use standard digital computers. Our calculations generate a distribution equivalent to the observables predicted by quantum mechanics. These results demonstrate the potential for phase-space methods to simulate macroscopic quantum superpositions.

We have demonstrated genuine multipartite Bell inequalities with up to 60 qubits. In all cases we have shown violations of these inequalities using positive phase space distributions. We are interested in the question of whether or not probabilistic sampling can be carried out for GHZ states. This is not obvious a-priori, since one might expect highly nonclassical states to be hard to sample probabilistically. We also have performed dynamical simulations of super-decoherence.

These results demonstrate that the simulation of both low and high order correlations is feasible, despite Bell violations. Some reasonable conclusions about the advantages and limitations of these methods are as follows. Probabilistic phase-space algorithms appear well suited to low order correlations, including fundamentally non-classical low order Bell inequality violations. Higher order correlations generate larger sampling errors with a probabilistic approach.

We also find a classical parallelism which gives an an unexpected exponential speed-up for qubit sampling, when calculating all the high order correlations required for multipartite Bell violations. Here the speed-up is relative to the corresponding experimental times, and is exponential in the qubit number. This uniquely useful feature of probabilistic phase-space methods is due to their ability to simultaneously calculate many non-commuting observables in parallel.

Such classical *measurement* parallelism is complementary to the *state* parallelism of quantum mechanics. We have utilized this in the calculation of the MABK function, to indicate genuine violation of multipartite Bell inequalities.

ACKNOWLEDGMENTS

We wish to acknowledge research funding from the Australian Research Council, as well as useful discussions with P. Deuar, R. Blatt and B. Lanyon.

-
- [1] P. A. M. Dirac, P. Roy. Soc. A. **123**, 714 (1929).
 - [2] R. P. Feynman, Int. J. Theor. Phys. **21**, 467 (1982).
 - [3] F. Haake, H. King, G. Schröder, J. Haus, and R. J. Glauber, Phys. Rev. A **20**, 2047 (1979).
 - [4] J. F. Corney *et al.*, Phys. Rev. Lett. **97**, 023606 (2006).
 - [5] P. P. Deuar and P. D. Drummond, Phys. Rev. Lett. **98**, 120402 (2007).
 - [6] O. E. Alon, A. I. Streltsov, and L. S. Cederbaum, Phys. Rev. A **77**, 033613 (2008).
 - [7] J. Gambetta *et al.*, Phys. Rev. A **77**, 012112 (2008).
 - [8] S. Trotzky *et al.*, Nat. Phys. **8**, 325 (2012).
 - [9] J. I. Cirac and P. Zoller, Science **301**, 176 (2003).
 - [10] D. Jaksch and P. Zoller, Ann. Phys. **315**, 52 (2005).
 - [11] I. Buluta and F. Nori, Science **326**, 108 (2009).
 - [12] R. Islam *et al.*, Nat. Commun. **2**, 377 (2011).
 - [13] I. M. Georgescu, S. Ashhab, and F. Nori, Rev. Mod. Phys. **86**, 153 (2014).
 - [14] B. P. Lanyon *et al.*, Science **334**, 57 (2011).
 - [15] R. J. Glauber and F. Haake, Phys. Lett. A **68**, 29 (1978).
 - [16] P. D. Drummond and C. W. Gardiner, J. Phys. A: Math. Gen. **13**, 2353 (1980).
 - [17] S. J. Carter, P. D. Drummond, M. D. Reid, and R. M. Shelby, Phys. Rev. Lett. **58**, 1841 (1987).
 - [18] M. Rosenbluh and R. M. Shelby, Phys. Rev. Lett. **66**, 153 (1991).
 - [19] P. D. Drummond, R. M. Shelby, S. R. Friberg, and Y. Yamamoto, Nature **365**, 307 (1993).
 - [20] J. Heersink, V. Josse, G. Leuchs, and U. L. Andersen,

- Opt. Lett. **30**, 1192 (2005).
- [21] R. J. Lewis-Swan and K. V. Kheruntsyan, Nat. Commun. **5**, 3752 (2014).
- [22] L. Rosales-Zárate, B. Opanchuk, P. D. Drummond, and M. D. Reid, (2014), arXiv:1405.1168.
- [23] D. M. Greenberger, M. A. Horne, and A. Zeilinger, *Bell's Theorem, Quantum Theory and Conceptions of the Universe*, edited by M. Kafatos (Springer, 1989) p. 348.
- [24] C.-Y. Lu *et al.*, Nat. Phys. **3**, 91 (2007).
- [25] D. Leibfried *et al.*, Nature **438**, 639 (2005).
- [26] B. P. Lanyon *et al.*, Phys. Rev. Lett. **112**, 100403 (2014).
- [27] N. D. Mermin, Phys. Rev. Lett. **65**, 1838 (1990).
- [28] Y. Aharonov, D. Z. Albert, and L. Vaidman, Phys. Rev. Lett. **60**, 1351 (1988).
- [29] P. D. Drummond, B. Opanchuk, L. E. C. Rosales-Zárate, and M. D. Reid, Phys. Scripta **T160**, 014009 (2014).
- [30] B. Opanchuk, L. E. C. Rosales-Zárate, M. D. Reid, and P. D. Drummond, Phys. Lett. A **378**, 946 (2014).
- [31] K. Husimi, Proc. Phys. Math. Soc. Jpn. **22**, 264 (1940).
- [32] F. Arecchi, E. Courtens, R. Gilmore, and H. Thomas, Phys. Rev. A **6**, 2211 (1972).
- [33] R. Gilmore, C. Bowden, and L. Narducci, Phys. Rev. A **12**, 1019 (1975).
- [34] P. D. Drummond, Phys. Rev. Lett. **50**, 1407 (1983).
- [35] M. Ardehali, Phys. Rev. A **46**, 5375 (1992).
- [36] A. V. Belinskiĭ and D. N. Klyshko, Phys-Usp. **36**, 653 (1993).
- [37] A. V. Belinsky and D. N. Klyshko, Phys. Lett. A **176**, 415 (1993).
- [38] G. Svetlichny, Phys. Rev. D **35**, 3066 (1987).
- [39] D. Collins, N. Gisin, S. Popescu, D. Roberts, and V. Scarani, Phys. Rev. Lett. **88**, 170405 (2002).
- [40] S. Ghose, N. Sinclair, S. Debnath, P. Rungta, and R. Stock, Phys. Rev. Lett. **102**, 250404 (2009).
- [41] A. Ajoy and P. Rungta, Phys. Rev. A **81**, 052334 (2010).
- [42] J.-D. Bancal, N. Brunner, N. Gisin, and Y.-C. Liang, Phys. Rev. Lett. **106**, 020405 (2011).
- [43] J.-L. Chen, D.-L. Deng, H.-Y. Su, C. Wu, and C. H. Oh, Phys. Rev. A **83**, 022316 (2011).
- [44] B. Grandjean, Y.-C. Liang, J.-D. Bancal, N. Brunner, and N. Gisin, Phys. Rev. A **85**, 052113 (2012).
- [45] R. F. Werner and M. M. Wolf, Phys. Rev. A **64**, 032112 (2001).
- [46] A. Einstein, B. Podolsky, and N. Rosen, Phys. Rev. **47**, 777 (1935).
- [47] N. D. Mermin, Phys. Today **43**, 9 (1990).
- [48] J. S. Bell, Physics **1**, 195 (1964).
- [49] J. F. Clauser, M. A. Horne, A. Shimony, and R. A. Holt, Phys. Rev. Lett. **23**, 880 (1969).
- [50] J. F. Clauser and A. Shimony, Rep. Prog. Phys. **41**, 1881 (1978).
- [51] B. D'Espagnat, ed., *Foundations of Quantum Mechanics* (Academic Press, New York, 1971).
- [52] M. Seevinck and G. Svetlichny, Phys. Rev. Lett. **89**, 060401 (2002).
- [53] L. Aolita, R. Gallego, A. Cabello, and A. Acín, Phys. Rev. Lett. **108**, 100401 (2012).
- [54] R. Gallego, L. E. Würflinger, A. Acín, and M. Navascués, Phys. Rev. Lett. **109**, 070401 (2012).
- [55] J.-D. Bancal, J. Barrett, N. Gisin, and S. Pironio, Phys. Rev. A **88**, 014102 (2013).
- [56] E. P. Wigner, Phys. Rev. **40**, 749 (1932).
- [57] R. J. Glauber, Phys. Rev. **131**, 2766 (1963).
- [58] E. Sudarshan, Phys. Rev. Lett. **10**, 277 (1963).
- [59] S. Chaturvedi, G. S. Agarwal, and V. Srinivasan, J. Phys. A: Math. Gen. **27**, L39 (1994).
- [60] F. A. M. de Oliveira, Phys. Rev. A **45**, 5104 (1992).
- [61] J. F. Corney and P. D. Drummond, Phys. Rev. A **68**, 063822 (2003).
- [62] J. M. Radcliffe, J. Phys. A: Gen. Phys. **4**, 313 (1971).
- [63] W.-M. Zhang, D. H. Feng, and R. Gilmore, Rev. Mod. Phys. **62**, 867 (1990).
- [64] D. W. Barry and P. D. Drummond, Phys. Rev. A **78**, 052108 (2008).
- [65] W. K. Wootters, Ann. Phys. **176**, 1 (1987).
- [66] W. K. Wootters and B. D. Fields, Ann. Phys. **191**, 363 (1989).
- [67] K. S. Gibbons, M. J. Hoffman, and W. K. Wootters, Phys. Rev. A **70**, 062101 (2004).
- [68] W. K. Wootters, IBM J. Res. Dev. **48**, 99 (2004).
- [69] W. K. Wootters, Found. Phys. **36**, 112 (2006).
- [70] G. Björk, A. B. Klimov, and L. L. Sánchez-Soto, Prog. Optics **51**, 469 (2008).
- [71] L. C. Biedenharn and H. van Dam, *Quantum theory of angular momentum: a collection of reprints and original papers* (Academic Press, New York, 1965) p. 332.
- [72] M. D. Reid and D. F. Walls, Phys. Rev. A **34**, 1260 (1986).
- [73] M. Brune *et al.*, Phys. Rev. Lett. **77**, 4887 (1996).
- [74] T. Monz *et al.*, Phys. Rev. Lett. **106**, 130506 (2011).